

Effects of VLSI Circuit Constraints on Temporal-Coding Multilayer Spiking Neural Networks ^{*}

Yusuke Sakemi¹[0000–0002–0274–9491], Takashi Morie²[0000–0003–2708–4307],
Takeo Hosomi¹[0000–0001–5972–3877], and Kazuyuki
Aihara^{3,4}[0000–0002–4602–9816]

¹ NEC Corporation, Kawasaki, Japan ysakemi@nec.com

² Graduate School of Life Science and Systems Engineering, Kyushu Institute of
Technology, Kitakyushu, Japan

³ Institute of Industrial Science, The University of Tokyo, Tokyo, Japan

⁴ International Research Center for Neurointelligence (WPI-IRCN), The University
of Tokyo Institutes for Advanced Study, The University of Tokyo, Tokyo, Japan

Abstract. The spiking neural network (SNN) has been attracting considerable attention not only as a mathematical model for the brain, but also as an energy-efficient information processing model for real-world applications. In particular, SNNs based on temporal coding are expected to be much more efficient than those based on rate coding, because the former requires substantially fewer spikes to carry out tasks. As SNNs are continuous-state and continuous-time models, it is favorable to implement them with analog VLSI circuits. However, the construction of the entire system with continuous-time analog circuits would be infeasible when the system size is very large. Therefore, mixed-signal circuits must be employed, and the time discretization and quantization of the synaptic weights are necessary. Moreover, the analog VLSI implementation of SNNs exhibits non-idealities, such as the effects of noise and device mismatches, as well as other constraints arising from the analog circuit operation. In this study, we investigated the effects of the time discretization and/or weight quantization on the performance of SNNs. Furthermore, we elucidated the effects the lower bound of the membrane potentials and the temporal fluctuation of the firing threshold. Finally, we propose an optimal approach for the mapping of mathematical SNN models to analog circuits with discretized time.

Keywords: spiking neural network · temporal coding · supervised learning · VLSI.

^{*} partially supported by the “Brain-Morphic AI to Resolve Social Issues” project at UTokyo, the NEC Corporation, AMED under Grant Number JP20dm0307009, and JST Moonshot R&D Grant Number JPMJMS2021.

1 Introduction

Spiking neural networks (SNNs) are expected to be energy-efficient models because they can process information in the form of spikes in an event-driven manner. Moreover, the performance of SNNs has been demonstrated to be comparable to that of artificial neural networks (ANNs) with deep learning in relatively small-scale image recognition tasks [21,18]. The information representations in SNNs can be approximately classified into two domains: rate and temporal coding. The information is contained in the rate of the spikes in rate coding, whereas it is contained in the precise timing of the spikes in temporal coding. Although rate coding is closely linked to ANNs [5][11] in which the neuron states are represented by analog values, temporal coding can efficiently exploit the information of the temporal dynamics of the membrane potentials and synaptic currents, which are not considered in ANNs [7]. In particular, time-to-first-spike (TTFS) coding, which is a type of temporal coding, is expected to be the most efficient because the information of a neuron output is represented as the timing of a single spike [2][16][3][19].

As SNNs are expressed as continuous-state and continuous-time systems, analog VLSI implementation is favorable. However, the construction of the entire system, including the input/output parts, would be infeasible with continuous-time analog circuits when the system size is very large because of inflexibility in system design and difficulty in analog circuit design. The discretization of the neuron activation in the time domain and quantization of the synaptic weights are required. Therefore, many studies on SNNs have adopted fully digital VLSI implementation [14][4] or mixed-signal VLSI implementation [15].

In this study, we temporally discretized SNNs trained with TTFS coding and quantized the synaptic weights to facilitate VLSI implementation. Moreover, we investigated the effects of the lower bound of the membrane potentials and the temporal fluctuation of the firing thresholds, which are problematic in analog VLSI implementation. Section 2 introduces related works, Section 3 presents the investigation into the above-mentioned effects, and Section 4 demonstrates the optimal mapping of SNNs to analog VLSI circuits.

2 Related works

Several supervised learning algorithms for multilayer SNNs based on temporal coding have been proposed in discrete time systems [8][10]. However, these algorithms require approximations to obtain the derivative of the spike timing with respect to the weights to derive the backpropagation algorithms. In our approach, the SNNs are trained in continuous time and then discretized, which does not require any approximation to derive the backpropagation algorithm apart from the spike vanishing problem [2], and therefore, the training of the SNNs is easier. Moreover, as we demonstrate later, the discretized time step for the spike timing is important to map the SNNs to VLSI circuits optimally. In our method, once the SNNs are trained in a continuous-time system, an arbitrary

time step can be selected for the spike timing without retraining, whereas in the other approaches, the optimization of the time step is difficult because the time step must be fixed when training SNNs [8][10]. Furthermore, we note that it is common to quantize the activation of neurons after training in ANNs [20].

Certain research groups have designed VLSI circuits for SNNs based on TTFS coding [6][17]. Göltz *et al.* designed a mixed-signal circuit and demonstrated SNNs based on TTFS coding [6]. Oh *et al.* designed analog SNN circuits with analog memory based on TTFS coding [17]. Although Kheradpishesh *et al.* [9] and Sakemi *et al.* [19] investigated the effects of the timing jitter of spikes on the performance, the effects of the time discretization of the spikes have not been discussed. Sakemi *et al.* [19] and Oh *et al.* [17] investigated the effects of fixed scattering of the firing thresholds owing to device mismatches. However, they did not discuss the effects of the temporal fluctuation of the firing thresholds. Oh *et al.* [17] investigated the effects of the variations in the synaptic weights, and Kheradpishesh *et al.* [9] binarized weights of SNNs on TTFS coding. However, they did not discuss the effects of weight quantization. To the best of our knowledge, the effects of the lower bound of the membrane potentials for SNNs based on TTFS coding have not been investigated in previous works [2][16][3][19][6][17].

3 Effects of non-idealities arising from VLSI circuit constraints

3.1 Models

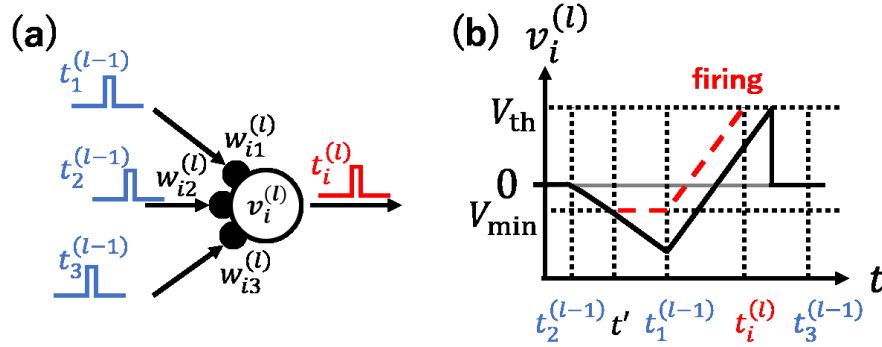


Fig. 1. (a) Schematic diagram of the i th neuron in the l th layer receiving spikes from neurons in the $l - 1$ th layer at $t_1^{(l-1)}$, $t_2^{(l-1)}$, $t_3^{(l-1)}$, and firing at $t_i^{(l)}$. (b) Schematic diagram of time evolution of the membrane potential of the i th neuron in the l th layer with (red dashed line) and without (black solid line) a lower bound of the membrane potential. The upper and lower horizontal black dotted lines represent the values of V_{th} and V_{min} , respectively.

We adopted a simple integrate-and-fire neuron model in a multilayer network that was suitable for VLSI implementation [13][19]:

$$\frac{d}{dt}v_i^{(l)}(t) = \sum_j^N w_{ij}^{(l)}\theta(t - t_j^{(l-1)}) \quad (1)$$

$$\theta(x) = \begin{cases} 0, & (x < 0) \\ 1, & (x \geq 0) \end{cases} \quad (2)$$

where $v_i^{(l)}(t)$ is the membrane potential of the i th neuron in the l th layer, $w_{ij}^{(l)}$ is the weight from the j th neuron in the $l - 1$ th layer to the i th neuron in the l th layer, and $t_j^{(l-1)}$ is the spike timing of the j th neuron in the $l - 1$ th layer. When the membrane potential exceeds the firing threshold V_{th} , the neuron generates a spike. Then, the membrane potential is set to 0 and the potential does not change again. Fig. 1 shows schematic diagram of the neuron model.

For image processing in SNNs, the normalized intensity of the i th pixel of an image $x_i \in (0, 1]$ is converted into an input spike, with the timing given by

$$t_i^{(0)} = \tau(1 - x_i) \quad (3)$$

where τ is the time span of the input spikes and it is set to 5 ms. When $x_i = 0$, the i th input spike is not generated. To improve the generalization ability, Gaussian noise was introduced into the timing of the input spikes in the training phase. The SNNs were trained with the backpropagation algorithm described in [19].

We investigated the following effects in the VLSI implementation of SNNs: (i) the discretization of the spike timing of the neurons, (ii) the quantization of the weights, (iii) the lower bound of the membrane potentials, and (iv) the temporal fluctuation of the firing threshold. In the remainder of this section, we explain the experimental setup used to investigate these effects. We note that training is performed offline, and only the inference is carried out on a VLSI circuit. Therefore, we did not consider effects (i) to (iv) when training the SNNs.

After training the SNNs, we discretized the timing of the spikes as follows:

$$t_i^{(l)} := T_{\text{clock}}^{(\text{model})} t_i^{(l, \text{step})} \quad (4)$$

$$t_i^{(l, \text{step})} := \min\{p \in \mathbb{Z} | v_i^{(l)}(T_{\text{clock}}^{(\text{model})} p) \geq V_{th}^{(\text{model})}\} \quad (5)$$

where $T_{\text{clock}}^{(\text{model})}$ is a positive real number representing the time step of the spike timing and $t_i^{(l, \text{step})}$ is an integer. The time-discretized spikes are sent to neurons in the subsequent layer. The synaptic weights $w_{ij}^{(l)}$ are replaced with the quantized weights $w^{(\min)} w_{ij}^{(l, \text{level})}$, where $w^{(\min)}$ is a positive real number and $w_{ij}^{(l, \text{level})}$ is an integer given by $\text{round}(w_{ij}^{(l)} / w^{(\min)})$.

The membrane potential provided by (1) can take any value less than V_{th} . However, the range of the membrane potential is limited in analog VLSI circuits. To investigate the effects of such a limited range, we modified the neuron

equation (1) so that the membrane potential could not take a value less than V_{\min} :

$$\frac{d}{dt}v_{ij}^{(l)}(t) = \begin{cases} 0, & \text{if } v_{ij}^{(l)}(t) = V_{\min} \text{ and } \sum_j^N w_{ij}^{(l)}\theta(t - t_j^{(l-1)}) < 0 \\ \sum_j^N w_{ij}^{(l)}\theta(t - t_j^{(l-1)}), & \text{otherwise.} \end{cases} \quad (6)$$

Fig. 1 (b) presents a schematic of the evolution of the membrane potential according to (6). The solid line represents the membrane potential when the lower bound of the membrane potential is not considered. The dashed line represents the membrane potential when the lower bound of the membrane potential is V_{\min} . In the latter case, the membrane potential is V_{\min} from time t' to time $t_1^{(l-1)}$, where the sum of the inputs $\sum_j^N w_{ij}^{(l)}\theta(t - t_j^{(l-1)})$ is less than 0. For $t > t_1^{(l-1)}$, where the sum of the inputs is positive, the membrane potential begins to increase. As a result, the spike timing $t_i^{(l)}$ when the lower bound is considered is different from the spike timing when the lower bound is not considered. We note that when V_{\min} is sufficiently low, the membrane potentials obtained by (6) converge to the membrane potentials obtained by (1).

Finally, to investigate the effects of the temporal fluctuation of the firing threshold, we modeled the firing threshold as a time-dependent function $V_{\text{th}}(t)$. The value of $V_{\text{th}}(t)$ is drawn from the Gaussian distribution as

$$V_{\text{th}}(i) \sim N(V_{\text{th}}, \sigma_{V_{\text{th}}}), \quad i = 0, 1, \dots \quad (7)$$

where $N(a, b)$ is a Gaussian distribution with a mean of a and standard deviation of b . The standard deviation of the firing threshold is given by $\sigma_{V_{\text{th}}}$.

3.2 Results

In this section, we demonstrate the effects of VLSI circuit constraints on SNNs (784-800-10) for the MNIST [12] and Fashion-MNIST [24] datasets.

Fig. 2 presents the timing of the spikes (raster plots) and time evolution of the membrane potentials for the MNIST dataset when $T_{\text{clock}}^{(\text{model})} = 2$ ms, $V_{\min} = -0.5$, and $\sigma_{V_{\text{th}}} = 0.04$. In the raster plot, the timing of the spikes lay only on integer numbers multiplied by $T_{\text{clock}}^{(\text{model})}$. The slope of the membrane potential changed only at time discretized by $T_{\text{clock}}^{(\text{model})}$. Moreover, the membrane potential never took values lower than V_{\min} .

The left panels of Fig. 3 depicts the performance of the SNNs with time-discretized spikes for various values of $T_{\text{clock}}^{(\text{model})}$. For both the MNIST and Fashion-MNIST datasets, the effects of the time discretization of the spikes at the output layer were more significant than those at the other layers. This can be attributed to the fact that the prediction results obtained by the network are represented by the earliest spike at the output layer. If the real timing difference between the earliest and second earliest spikes is less than $T_{\text{clock}}^{(\text{model})}$, the network cannot predict the correct label when the timing of the spikes is discretized. The effects of the time discretization of the spike timing were substantially lower for the

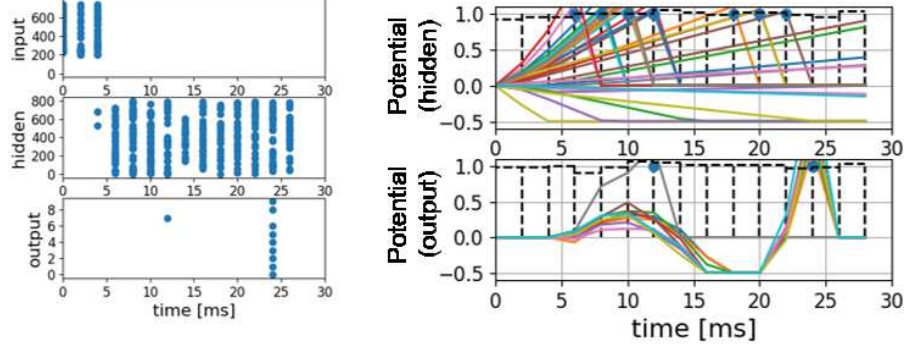


Fig. 2. Typical results of raster plots (left panels) and membrane potentials (right panels) for MNIST dataset. $T_{clock}^{(model)} = 2$ ms, $V_{min} = -0.5$, and $\sigma_{V_{th}} = 0.04$. Weights are not quantized. The horizontal dashed lines in the right panels represent the values of the temporally fluctuating firing threshold V_{th} .

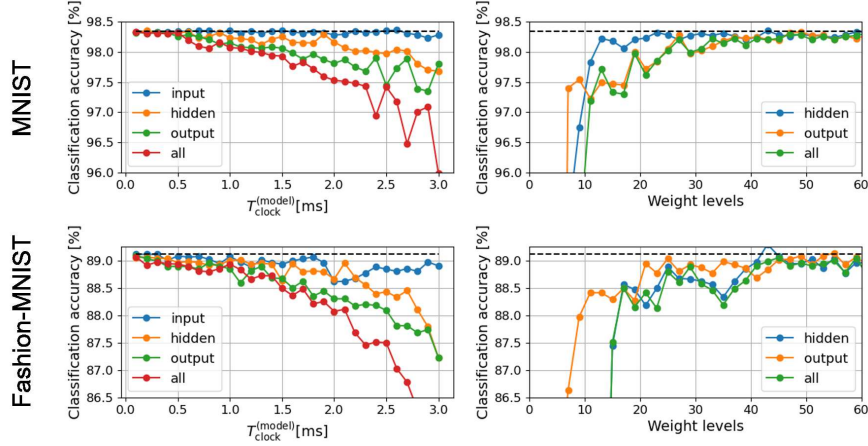


Fig. 3. Classification accuracy of SNNs on MNIST and Fashion-MNIST datasets with time-discretization (left panels) and weight quantization (right panels). The horizontal dashed lines in all panels represent the performance when no circuit constraints are considered.

input layer. This may be because the coding of the input spikes includes “no spike” states, which are inherently robust against timing discretization.

The right panels of Fig. 3 presents the performance of the SNNs when the weights were quantized. In this figure, the horizontal axis represents the number of levels of the quantized weights, given by $\max(|w_{ij}^{(l)}|)/w^{(\min)}$. We found that performance degradation could be avoided if the number of levels was greater than approximately 20.

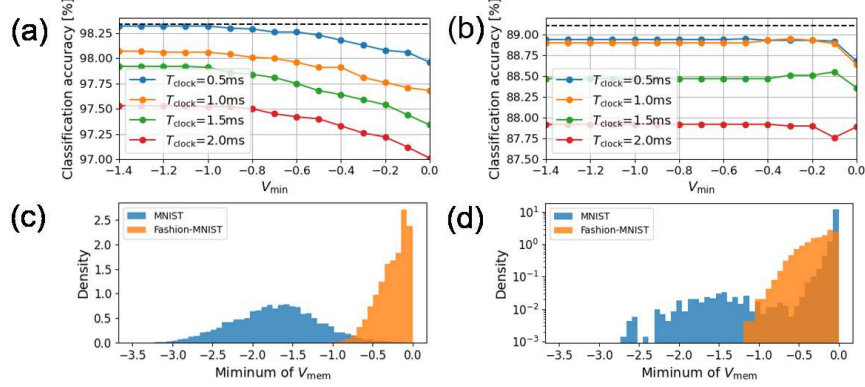


Fig. 4. Classification accuracy for various values of lower bound V_{\min} of membrane potential for (a) MNIST dataset and (b) Fashion-MNIST dataset. The distributions of the lowest membrane potentials in the output layer (c) and those of the lowest membrane potential before the earliest timing of spikes in the output layer (d) when $T_{\text{clock}}^{(\text{model})} = 0.6$ ms for the above datasets. The horizontal dashed lines in (a) and (b) represent the performance when no circuit constraints are considered.

Figs. 4 (a) and (b) present the classification accuracy for various values of the lower bound V_{\min} of the membrane potential. Fig. 4 (c) shows the distribution of the minimum value of the membrane potential of the neurons at the output layer, given by

$$v^{(\min)} := \min_i \left(\min_{t < t_i^{(2)}} v_i^{(2)}(t) \right) \quad (8)$$

when V_{\min} was not considered. Because the membrane potentials were more likely to take lower values for the MNIST dataset than for the Fashion-MNIST dataset, the SNNs trained on the MNIST dataset were more vulnerable to the value of V_{\min} as indicated in Figs. 4 (a) and (b). We note that the performance was not affected when only the lower bound the membrane potential of neurons in the hidden layer were considered.

One may wonder why the SNNs trained on the MNIST dataset were almost not affected by the lower bound when $V_{\min} = -1$, even though the average of

the minimum voltage $v^{(\min)}$ given by (8) was much lower than -1 as shown in Fig. 4 (c). This is because the minimum values (8) were typically obtained after another neuron was fired, as shown in Fig. 2. To elucidate this fact, Fig. 4 (d) plots the distribution of the minimum membrane potential before the timing of the earliest spike:

$$\hat{v}^{(\min)} := \min_i \left(\min_{t < \min_j t_j^{(2)}} v_i^{(2)}(t) \right). \quad (9)$$

We found that a large portion of the minimum membrane potentials given by (9) had distributions that were higher than -0.5.

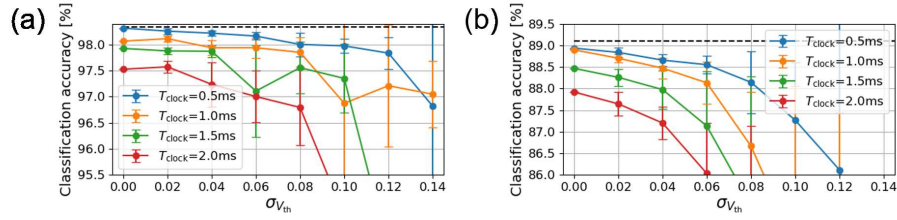


Fig. 5. Classification accuracy for various values of $\sigma_{V_{th}}$ for (a) MNIST dataset and (b) Fashion-MNIST dataset. The horizontal dashed lines in (a) and (b) represent the performance when any circuit constraints are not considered.

Fig. 5 depicts the classification accuracy for various values of $\sigma_{V_{th}}$. We found that the performance of the SNNs was not significantly impaired if $\sigma_{V_{th}}$ was less than 0.05 for the MNIST and Fashion-MNIST datasets.

4 Mapping of SNNs to VLSI circuits

We demonstrate a procedure for mapping SNNs to VLSI circuits. First, we introduce a VLSI circuit model derived from Kirchhoff's law. Second, we show how to map an SNN to the VLSI circuit optimally, assuming certain circuit parameters and constraints.

4.1 Circuit model

We consider an integrate-and-fire model as illustrated in Fig. 6, which is commonly employed in matrix-vector computation [23][22][1][25] and SNNs [19,17]. The time evolution of the membrane potential represented by the voltage at a capacitor is obtained by Kirchhoff's current law, as follows:

$$C \frac{d}{dt} v_i^{(l)}(t) = I^{(\min)} \sum_j^N I_{ij}^{(\text{level})} \theta(t - t_j^{(l-1)}) \quad (10)$$

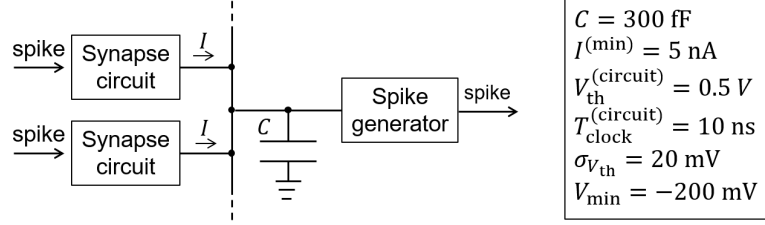


Fig. 6. Schematic of integrate-and-fire neuron circuit. Currents from many synapses are converted into voltage at the capacitor C . A spike is generated when the voltage exceeds a threshold.

where $I^{(\min)}$ represents the controllable minimum current, $I_{ij}^{(\text{level})}$ is an integer, and C is the capacitance. The timing of the firing is obtained as follows:

$$t_i^{(l)} := T_{\text{clock}}^{(\text{circuit})} t_i^{(l, \text{step})} \quad (11)$$

$$t_i^{(l, \text{step})} = \min\{p \in \mathbb{Z} | v_i^{(l)}(T_{\text{clock}}^{(\text{circuit})} p) \geq V_{\text{th}}^{(\text{circuit})}\} \quad (12)$$

where $T_{\text{clock}}^{(\text{circuit})}$ is a real number representing the time step of the time-discrete spikes in the circuits.

By setting $I_{ij}^{(l, \text{level})} = w_{ij}^{(l, \text{level})}$, the condition whereby (1) and (10) are equivalent can be obtained as follows:

$$T_{\text{clock}}^{(\text{model})} w^{(\min)} = \frac{T_{\text{clock}}^{(\text{circuit})} I^{(\min)} V_{\text{th}}^{(\text{model})}}{C V_{\text{th}}^{(\text{circuit})}}. \quad (13)$$

4.2 Optimal mapping of SNNs to circuits

We used the circuit parameters displayed in Fig. 6 to study the mapping of SNNs to circuits. These values of parameters were determined typically from VLSI design based on the approach of time-domain analog computing with transient states (TACT), in which synapse currents were given by field-effect transistors operating in a subthreshold region [22,25].

Fig. 7 presents the classification accuracy for various values of $T_{\text{clock}}^{(\text{model})}$. Note that the value of $w^{(\min)}$ was determined using the values of $T_{\text{clock}}^{(\text{model})}$ and (13). For the MNIST dataset, the classification accuracy decreased almost monotonically as $T_{\text{clock}}^{(\text{model})}$ increased. For the Fashion-MNIST dataset, the classification accuracy exhibited a peak around $T_{\text{clock}}^{(\text{model})} = 0.4$ ms. The performance of the SNN was mainly affected by the time discretization and weight quantization. To elucidate that, Fig. 7 also depicts the classification accuracy when only the time discretization and the weight quantization were considered and that when only the time discretization or the weight quantization was considered.

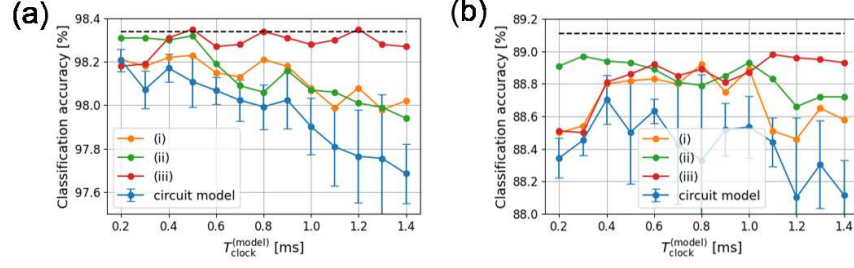


Fig. 7. Classification accuracy on (a) MNIST dataset and (b) Fashion-MNIST dataset with circuit model for various values of $T_{\text{clock}}^{(\text{model})}$. Classification accuracy is depicted when the circuit model is considered, (i) when only the effects of time discretization and weight quantization are considered, (ii) when only the effects of time discretization is considered, and (iii) when only the effects of weight quantization is considered. Note that the effects of the lower bound of the membrane potential and the temporal fluctuation of firing threshold are not included in (i)-(iii). The horizontal dashed lines in (a) and (b) represent the performance when no circuit constraints are considered.

As the network could cease its operation after the earliest spike was generated in the output layer, the energy efficiency increased as the average timing of the earliest spike became shorter. Fig. 8 indicates that the average timing of the earliest spike at the output layer decreased as a function of $T_{\text{clock}}^{(\text{model})}$, because the time steps required to obtain the output spikes was small when $T_{\text{clock}}^{(\text{model})}$ was large (see Fig. 2) with the same $T_{\text{clock}}^{(\text{circuit})}$.

The optimal choice of $T_{\text{clock}}^{(\text{model})}$ was determined by the trade-off between the classification accuracy (Fig. 7) and energy efficiency (Fig. 8). For example, if an accuracy of more than 98% was required with the minimum energy efficiency for the MNIST dataset, the optimal $T_{\text{clock}}^{(\text{model})}$ would be approximately 0.8 ms.

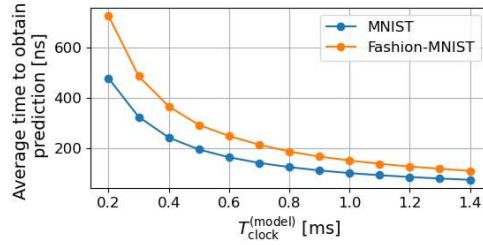


Fig. 8. Average time of earliest spike at output layer for various values of $T_{\text{clock}}^{(\text{model})}$.

5 Conclusions

In this study, we evaluated the performance of SNNs with TTFS coding on the MNIST and Fashion-MNIST datasets when considering circuit constraints. We found that the SNNs with TTFS coding were robust against these circuit constraints. Although information is contained in the precise spike timing in SNNs, the performance of the SNNs was only slowly degraded as the time step of the time discretization increased. Only 20 or 30 quantized levels were sufficient for the weights to prevent performance impairment, which corresponded to 4- or 5-bit precision. The lower bound of the membrane potential was not critical if we used only the earliest spike as the prediction result. The temporal fluctuation of the firing threshold was also not critical.

We demonstrated the optimal mapping of SNN models with TTFS coding to VLSI circuits, assuming a reasonable set of circuit parameters. We confirmed that the optimal choice of the discretization parameters for the spike timing and weights is obtained by a trade-off between the classification accuracy and energy efficiency. In this study, we fixed the circuit parameters and searched for the optimal discretization parameters for the SNNs. It will be straightforward to expand this strategy so that one can also search for optimal circuit parameters such as the clock period $T_{\text{clock}}^{(\text{circuit})}$ and the capacitance of neurons C . Further, we focused on a specific neuron model (1), however, the proposed techniques can be applied to other neuron models such as ones adopted in [16] and [3].

Acknowledgment

The authors would like to thank Kazumasa Yanagisawa and Masatoshi Yamaguchi from Floadia corporation for the fruitful discussion.

References

1. Bavandpour, M., Mahmoodi, M.R., Strukov, D.B.: Energy-efficient time-domain vector-by-matrix multiplier for neurocomputing and beyond. *IEEE Transactions on Circuits and Systems II: Express Briefs* (2019)
2. Bohte, S.M., Kok, J.N., Poutré, H.L.: Error-backpropagation in temporally encoded networks of spiking neurons. *Neurocomputing* **48**(1), 17–37 (October 2002)
3. Comsa, I.M., et al.: Temporal coding in spiking neural networks with alpha synaptic function. In: *ICASSP 2020 - 2020 IEEE International Conference on Acoustics, Speech and Signal Processing (ICASSP)*. pp. 8529–8533 (2020)
4. Davies, M., et al.: Loihi: A neuromorphic manycore processor with on-chip learning. *IEEE Micro* **38**(1), 82–99 (2018)
5. Diehl, P.U., et al.: Fast-classifying, high-accuracy spiking deep networks through weight and threshold balancing. In: *2015 International Joint Conference on Neural Networks (IJCNN)*. pp. 1–8 (July 2015)
6. Göltz, J., et al.: Fast and deep neuromorphic learning with first-spike coding. In: *Proceedings of the Neuro-inspired Computational Elements Workshop*. pp. 1–3 (2020)

7. Huh, D., Sejnowski, T.J.: Gradient descent for spiking neural networks. In: *Advances in Neural Information Processing Systems*. vol. 31, pp. 1433–1443 (2018)
8. Kheradpisheh, S.R., Masquelier, T.: Temporal backpropagation for spiking neural networks with one spike per neuron. *International Journal of Neural Systems* **30**(6), 2050027 (2020)
9. Kheradpisheh, S.R., Mirsadeghi, M., Masquelier, T.: BS4NN: Binarized spiking neural networks with temporal coding and learning. arXiv:2007.04039 (2020)
10. Kim, J., Kim, K., Kim, J.J.: Unifying activation-and timing-based learning rules for spiking neural networks. arXiv:2006.02642 (2020)
11. Kim, S., Park, S., Na, B., Yoon, S.: Spiking-YOLO: spiking neural network for energy-efficient object detection. In: *Proceedings of the AAAI Conference on Artificial Intelligence*. vol. 34, pp. 11270–11277 (2020)
12. LeCun, Y., Bottou, L., Bengio, Y., Haffner, P.: Gradient-based learning applied to document recognition. *Proceedings of the IEEE* **86**(11), 2278–2324 (November 1998)
13. Maass, W.: “Computing with Spiking Neurons,” in *Pulsed Neural Networks*, chap. 2, pp. 55–85. MIT Press (1999)
14. Merolla, P.A., et al.: A million spiking-neuron integrated circuit with a scalable communication network and interface. *Science* **345**(6197), 668–673 (2014)
15. Moradi, S., Qiao, N., Stefanini, F., Indiveri, G.: A scalable multicore architecture with heterogeneous memory structures for dynamic neuromorphic asynchronous processors (DYNAPs). *IEEE Transactions on Biomedical Circuits and Systems* **12**(1), 106–122 (Feb 2018)
16. Mostafa, H.: Supervised learning based on temporal coding in spiking neural networks. *IEEE Transactions on Neural Networks and Learning Systems* **29**(7), 3227–3235 (July 2018)
17. Oh, S., et al.: Hardware implementation of spiking neural networks using time-to-first-spike encoding. arXiv:2006.05033 (2020)
18. Pfeiffer, M., Pfeil, T.: Deep learning with spiking neurons: Opportunities and challenges. *Frontiers in Neuroscience* **12**(774), 1–18 (2018)
19. Sakemi, Y., Morino, K., Morie, T., Aihara, K.: A supervised learning algorithm for multilayer spiking neural networks based on temporal coding toward energy-efficient VLSI processor design. arXiv:2001.05348 (2020)
20. Sze, V., Chen, Y., Yang, T., Emer, J.S.: Efficient processing of deep neural networks: A tutorial and survey. *Proceedings of the IEEE* **105**(12), 2295–2329 (2017)
21. Tavanaei, A., Ghodrati, M., Kheradpisheh, S.R., Masquelier, T., Maida, A.: Deep learning in spiking neural networks. *Neural Networks* **111**, 47–63 (2019)
22. Wang, Q., Tamukoh, H., Morie, T.: A time-domain analog weighted-sum calculation model for extremely low power VLSI implementation of multi-layer neural networks. arXiv:1810.06819 (2018)
23. Wang, Q., Tamukoh, H., Morie, T.: Time-domain weighted-sum calculation for ultimately low power VLSI neural networks. In: *Neural Information Processing*. vol. 9947, pp. 240–247 (September 2016)
24. Xiao, H., Rasul, K., Vollgraf, R.: Fashion-MNIST: a novel image dataset for benchmarking machine learning algorithms. arXiv:1708.07747 (2017)
25. Yamaguchi, M., Iwamoto, G., Nishimura, Y., Tamukoh, H., Morie, T.: An energy-efficient time-domain analog cmos binaryconnect neural network processor based on a pulse-width modulation approach. *IEEE Access* **9**, 2644–2654 (2020)